

Randomized Dynamic Mode Decomposition for Non-Intrusive Reduced Order Modelling

D.A. Bistrian^{1*} and I.M. Navon²

¹*Department of Electrical Engineering and Industrial Informatics, Politehnica University of Timisoara, 331128 Hunedoara, Romania,*

²*Department of Scientific Computing, Florida State University, Tallahassee, FL, 32306-4120, USA*

SUMMARY

This paper focuses on a new framework for reduced order modelling of non-intrusive data with application to 2D flows. To overcome the shortcomings of intrusive model order reduction usually derived by combining the POD and the Galerkin projection methods, we developed a novel technique based on Randomized Dynamic Mode Decomposition as a fast and accurate option in model order reduction of non-intrusive data originating from Saint-Venant systems. Combining efficiently the Randomized Dynamic Mode Decomposition algorithm with Radial Basis Function interpolation, we produced an efficient tool in developing the linear model of a complex flow field described by non-intrusive (or experimental) data. The rank of the reduced DMD model is given as the unique solution of a constrained optimization problem. We emphasize the excellent behavior of the non-intrusive reduced order models by performing a qualitative analysis. In addition, we gain a significantly reduction of CPU time in computation of the reduced order models (ROMs) for non-intrusive numerical data.
Copyright © 2016 John Wiley & Sons, Ltd.

Received ...

KEY WORDS: dynamic mode decomposition; non-intrusive reduced order modelling; randomized SVD.

1. INTRODUCTION, FOCUS AND MOTIVATION

The current line of this survey is motivated by the efficiency of reduced order modelling in different problems arising in hydrodynamics, where data are collected in the aftermath of an experiment or are provided by measurement tools. We refer to this data as non-intrusive data. In the context of application of mathematical and numerical techniques for modelling the non-intrusive massive data, the intent of this paper is to undertake an efficient technique of model order reduction of shallow water systems. The challenge of this task is to build a linear dynamical system that models the evolution of the strongly nonlinear flow and to define a new mathematical and numerical methodology for studying dominant and coherent structures in the flow.

Among several model order reduction techniques, Proper Orthogonal Decomposition (POD) and Dynamic Mode Decomposition (DMD) represent modal decomposition methods that are widely applied to study dynamics in different applications. The application of POD is primarily limited to flows whose coherent structures can be hierarchically ranked in terms of their energy content. But there are situations when the energy content is not a sufficient criterion to accurately describe the dynamical behavior of the flows. Instead, DMD links the dominant flow features by a representation in the amplitudes-temporal dominant frequencies space.

*Correspondence to: Revolutiei Str. Nr.5, 331128 Hunedoara, Romania. E-mail: diana.bistrian@upt.ro

Current literature has explored a broad variety of applications of reduced order modelling (ROM). Recently, the POD approach has been incorporated for model order reduction purposes (MOR) by Chevreuil and Nouy [1], Stefanescu and Navon [2], Dimitriu et al. [3], Xiao et al. [4], Du et al. [5], Fang et al. [6]. POD proved to be an effective technique embedded also in inverse problems, as it was demonstrated by the work of Cao et al. [7, 8], Chen et al. [9], Stefanescu et al. [10], thermal analysis (Bialecki et al. [11]), non-linear structural dynamics problems (Carlberg et al. [12]) and aerodynamics (see for reference the recent work of Semaan and his coworkers [13]). The method of Dynamic Mode Decomposition is rooted in the theory of Krylov subspaces [14, 15, 16] due to the original derivation of DMD as a variant of the Arnoldi algorithm [17] and was first introduced in 2008 by Schmid and Sesterhenn [18]. Only a year later, Rowley et al. [15] presented their theory of Koopman spectral analysis, which has its inception back in 1931 [19]. In Dynamic Mode Decomposition, the modes are not orthogonal, but one advantage of DMD compared to POD is that each DMD mode is associated with a pulsation, a growth rate and each mode has a single distinct frequency. Owing to this feature, DMD method was used as a modal decomposition tool in non-linear dynamics (Schmid et al. [20], Noack et al. [21]), in fluid mechanics (Bagheri [22], Rowley et al. [23], Frederich and Luchtenburg [24], Alekseev et al. [25]) and was recently introduced in turbulent flow problems (Seena and Sung [26] and Hua et al. [27]). The theory of dynamic mode decomposition was applied for the purposes of model reduction within the efforts of Mezić [28, 29] and in flow control problems by Bagheri [30] and Brunton et al. [31]. For a complete description of the utility of DMD vs. POD for model reduction in shallow water problems, the reader is referred to our previous paper (Bistran and Navon [32]).

The Saint-Venant system is employed in the present research to provide the experimental data. The Saint-Venant equations, named after the French mathematician Adhémar Jean Claude Barré de Saint-Venant (1797 – 1886) (also called in literature the shallow-water equations (SWE)), are a set of hyperbolic partial differential equations that describe the flow below a pressure surface in a fluid. A description of the Saint-Venant system has been presented by Vreugdenhil [33], as a result of depth-integration of the Navier-Stokes equations [34]. In literature, SWE are used in various forms to describe hydrological and geophysical fluid dynamics phenomena. The shallow water magnetohydrodynamic (SWMHD) system has been devised by Gilman [35] to analyse the thin layer evolution of the solar tachocline. Recently, a wave relaxation solver for SWMHD has been developed by Bouchut and Lhébrard [36]. A collection of mathematical models in coastal engineering based on SWE have been developed by Koutitus [37], while a reduced order modeling of the upper tropical Pacific ocean has been presented by Cao et al. [7].

The intrusive model order reduction is usually derived by combining the POD and the Galerkin projection methods [32]. This approach suffers from efficiency issues because the Galerkin projection is mathematically performed by laborious calculation and requires stabilization techniques in the process of numerical implementation, as it was argued in [38, 39, 40].

The aim of this work is to circumvent these shortcomings by embedding the randomized dynamic mode decomposition as a fast and accurate option in model order reduction of non-intrusive data originating from Saint-Venant systems. We propose in this work a novel approach to derive a non-intrusive reduced order linear model of the flow dynamics (denoted as NIROM) based on Dynamic Mode Decomposition of experimental data in association with Radial Basis Function (RBF) multi-dimensional interpolation [17]. Several key innovations are introduced in this paper for the DMD-based model order reduction. The first one is represented by the randomization of the experimental data snapshots prior to singular value decomposition of matrix data. Thus, we endow the DMD algorithm with a randomized SVD algorithm aiming to improve the accuracy of the reduced order linear model and to reduce the CPU elapsed time. We gain a fast and accurate randomized DMD algorithm, exploiting an efficient low-rank DMD model of input data. The rank of the reduced DMD model represents the unique solution of an optimization problem whose constraints are a sufficiently small relative error of data reconstruction and a sufficiently high correlation coefficient between the experimental data and the DMD solution.

We recall this procedure as adaptive randomized dynamic mode decomposition (ARDMD).

The first major advantage of the adaptive randomized DMD proposed in this work is represented by the fact that the algorithm produces a reduced order subspace of Ritz values, having the same dimension as the rank of randomized SVD function. In consequence, a further selection algorithm of the Ritz values associated with their DMD modes is no longer needed. We employ in the flow reconstruction the smallest number of the DMD modes and their amplitudes and Ritz values, respectively, leading to the minimum error of flow reconstruction, due to the adaptive feature of the proposed algorithm. The second major improvement offered by the proposed randomized DMD can be found in the significantly reduction of CPU time for computation of massive numerical data.

A randomized SVD algorithm was recently employed in conjunction with dynamic mode decomposition in [41] for processing of high resolution videos in real-time. We believe that the present paper is the first work that shows the benefits of an efficient randomized dynamic mode decomposition algorithm with application in fluid dynamics.

The reminder of the article is organized as follows. In Section 2 we recall the principles governing the Dynamic Mode Decomposition and we provide the description of the DMD algorithm employed for decomposition of numerical data. In particular, we discuss the implementation of the randomized DMD for optimal selection of the low order model rank. Section 3 is dedicated to theoretical considerations about multidimensional radial basis functions interpolation. A detailed evaluation of the proposed numerical technique is presented in Section 4. Summary and conclusions are drawn in the final section.

2. ADAPTIVE RANDOMIZED DYNAMIC MODE DECOMPOSITION FOR NON-INTRUSIVE DATA

2.1. Koopman operator-the root of dynamic mode decomposition

Being rooted in the work of French-born American mathematician Bernard Osgood Koopman [19], the Koopman operator is applied to a dynamical system evolving on a manifold \mathbb{M} such that, for all $v_k \in \mathbb{M}$, $v_{k+1} = f(v_k)$, and it maps any scalar-valued function $g : \mathbb{M} \rightarrow \mathbb{R}$ into a new function $\mathcal{A}g$ given by

$$\mathcal{A}g(v) = g(f(v)). \quad (1)$$

Has been demonstrated yet that spectral properties of the flow will be contained in the spectrum of the Koopman operator [22] and even when f is finite-dimensional and nonlinear, the Koopman operator \mathcal{A} is infinite-dimensional and linear [15, 29]. There is a unique expansion that expands each snapshot in terms of vector coefficients ϕ_j which are called Koopman modes and mode amplitudes $a_j(w)$, such that iterates of v_0 are then given by

$$g(v_k) = \sum_{j=1}^{\infty} \lambda_j^k a_j(v_0) \phi_j, \quad \lambda_j = e^{\sigma_j + i\omega_j}, \quad (2)$$

where λ_j are called the Ritz eigenvalues of the modal decomposition, that are complex-valued flow structures associated with the growth rate σ_j and the frequency ω_j . Koopman modes represent spatial flow structures with time-periodic motion which are optimal in resolving oscillatory behavior. They have been increasingly used because they provide a powerful way of analysing nonlinear flow dynamics using linear techniques (see e.g. the work of Bagheri [22], Mezic [29], Rowley et al. [15]). The Koopman modes are extracted from the data snapshots and a unique frequency is associated to each mode. This is of major interest for fluid dynamics applications where phenomena occurring at different frequencies must be individualized.

A stable and consistent algorithm proposed by Schmid [16], referred in the literature as dynamic mode decomposition (DMD), can be used for computing approximately a subset of the Koopman spectrum from the time series of snapshots of the flow. Thus DMD generalizes the global stability modes and approximates the eigenvalues of the Koopman operator. The quantitative capabilities of DMD have already been well demonstrated in the literature and several DMD procedures have been released by the efforts of Rowley et al. [15], Schmid [16], Bagheri [22], Mezic [29], Belson et al. [42], Williams et al. [43].

Employing numerical simulations or experimental measurements techniques, different quantities associated with the flow are measured and collected as observations at one or more time signals, called observables or non-intrusive data. It turns out (see the survey of Bagheri [30]) that monitoring an observable over a very long time interval allows the reconstruction of the flow phase space. Assuming that $\{v_0, v_1, \dots, v_N\}$ is a data sequence collected at a constant sampling time Δt , the DMD algorithm is based on the hypothesis that a Koopman operator \mathcal{A} exists, that steps forward in time the snapshots, such that the snapshots data set

$$\{v_0, \mathcal{A}v_0, \mathcal{A}^2v_0, \dots, \mathcal{A}^{N-1}v_0\} \quad (3)$$

corresponds to the N^{th} Krylov subspace generated by the Koopman operator from v_0 . The goal of DMD is to determine eigenvalues and eigenvectors of the unknown matrix operator \mathcal{A} , thus a Galerkin projection of \mathcal{A} onto the subspace spanned by the snapshots is performed. For a sufficiently long sequence of the snapshots, we suppose that the last snapshot v_N can be written as a linear combination of previous $N - 1$ vectors, such that

$$v_N = c_0v_0 + c_1v_1 + \dots + c_{N-1}v_{N-1} + \mathcal{R}, \quad (4)$$

in which $c_i, i = 0, \dots, N - 1$ are complex numbers and \mathcal{R} is the residual vector. We assemble the following relations

$$\mathcal{A}\{v_0, v_1, \dots, v_{N-1}\} = \{v_1, v_2, \dots, v_N\} = \{v_1, v_2, \dots, V_0^{N-1}c\} + \mathcal{R}e_{N-1}^T, \quad (5)$$

where $V_0^{N-1} = \begin{pmatrix} v_0 & v_1 & \dots & v_{N-1} \end{pmatrix}$, $c^T = \begin{pmatrix} c_0 & c_1 & \dots & c_{N-1} \end{pmatrix}$ is the unknown complex column vector and e_j^T represents the j^{th} Euclidean unitary vector of length $N - 1$.

In matrix notation form, Eq. (5) reads

$$\mathcal{A}V_0^{N-1} = V_0^{N-1}\mathcal{C} + \mathcal{R}e_{N-1}^T, \quad \mathcal{C} = \begin{pmatrix} 0 & \dots & 0 & c_0 \\ 1 & & 0 & c_1 \\ \vdots & \vdots & \vdots & \vdots \\ 0 & \dots & 1 & c_{N-1} \end{pmatrix}, \quad (6)$$

where \mathcal{C} is the companion matrix.

A direct consequence of (6) is that decreasing the residual increases overall convergence and therefore the eigenvalues of the companion matrix \mathcal{C} will converge toward the eigenvalues of the Koopman operator \mathcal{A} .

The representation of data in terms of Dynamic Mode Decomposition is given by the linear model

$$v_{DMD}^t(\mathbf{x}) = \sum_{j=1}^k a_j \phi_j(\mathbf{x}) \lambda_j^{t-1}, \quad \lambda_j = e^{(\sigma_j + i\omega_j)\Delta t}, \quad t = t_1, \dots, t_N, \quad (7)$$

where the right eigenvectors $\phi_j \in \mathbb{C}$ are dynamic (Koopman) modes, the eigenvalues λ_j are called Ritz values [44] and coefficients $a_j \in \mathbb{C}$ are denoted as amplitudes or Koopman eigenfunctions. Each Ritz value λ_j is associated with the growth rate $\sigma_j = \frac{\log(|\lambda_j|)}{\Delta t}$ and the frequency $\omega_j = \frac{\arg(|\lambda_j|)}{\Delta t}$ and k represents the number of DMD modes involved in reconstruction.

Since it was first introduced in 2008 by Schmid and Sesterhenn [18], a considerable amount of work has focused on understanding and improving the method of dynamic mode decomposition. Chen et al. [14] introduced an optimized DMD, which tailors the decomposition to an optimal number of modes. This method minimizes the total residual over all data vectors and uses simulated annealing and quasi-Newton minimization iterative methods for selecting the optimal frequencies. A recursive dynamic mode decomposition was developed by Noack et al. [45] with application to a transient cylinder wake. Multi-Resolution DMD was released by Kutz et al. [46] for extracting DMD eigenvalues and modes from data sets containing multiple timescales. Efficient post processing procedures for selection of the most influential DMD modes and eigenvalues were presented in our previous papers [32, 47].

So far we have noticed two directions in developing the algorithms for dynamic mode decomposition. The straight-forward approach is seeking the companion matrix \mathcal{C} from (6) that helps to construct in a least squares sense the final data vector as a linear combination of all previous data vectors [15, 48, 23]. Because this version may be ill-conditioned in practice, Schmid [16] recommends an alternate algorithm, based on Singular Value Decomposition (SVD) [17] of snapshot matrix, upon which the work within this article is based.

2.2. Adaptive randomized DMD algorithm

To derive the improved algorithm proposed here, we proceed by collecting data $v_i(t, \mathbf{x}) = v(t_i, \mathbf{x})$, $t_i = i\Delta t$, $i = 0, \dots, N$, \mathbf{x} representing the spatial coordinates whether Cartesian or Cylindrical and form the snapshot matrix $V = \begin{bmatrix} v_0 & v_1 & \dots & v_N \end{bmatrix}$.

We arrange the snapshot matrix into two matrices. A matrix V_0^{N-1} is formed with the first N columns and the matrix V_1^N contains the last N columns of V : $V_0^{N-1} = \begin{bmatrix} v_0 & v_1 & \dots & v_{N-1} \end{bmatrix}$, $V_1^N = \begin{bmatrix} v_1 & v_2 & \dots & v_N \end{bmatrix}$.

Expressing V_1^N as a linear combination of the independent sequence V_0^{N-1} yields:

$$V_1^N = \mathcal{A}V_0^{N-1} = V_0^{N-1}\mathcal{S} + R,$$

where R is the residual matrix and \mathcal{S} approximates the eigenvalues of \mathcal{A} when $\|R\|_2 \rightarrow 0$. The objective at this step is to solve the minimization problem

$$\underset{\mathcal{S}}{\text{Minimize}} \quad R = \|V_1^N - V_0^{N-1}\mathcal{S}\|_2. \quad (8)$$

An estimate can be computed by multiplying V_1^N by the Moore-Penrose pseudoinverse of V_0^{N-1} :

$$\mathcal{S} = (V_0^{N-1})^+ V_1^N = W\Sigma^+ U^H V_1^N = X\Lambda X^{-1}, \quad (9)$$

where X and Λ represent the eigenvectors, respectively the eigenvalues of \mathcal{S} , and Σ^+ is computed according to Moore-Penrose pseudoinverse definition of Golub and van Loan [17]:

$$\Sigma^+ = \text{diag}\left(\frac{1}{\sigma_1}, \dots, \frac{1}{\sigma_r}, 0, \dots, 0\right), \quad r = \text{rank}(V_0^{N-1}). \quad (10)$$

It can be seen that the SVD plays a central role in computing the DMD. Therefore, this approach for computing the operator \mathcal{S} previously employed in [32] might not be feasible when dealing with high dimensional non-intrusive data. It is more desirable to reduce the problem dimension to avoid a computationally expensive SVD. Several key innovations are introduced in this paper for the DMD-based model order reduction.

First one is represented by the randomization of the experimental data matrix V_0^{N-1} prior to singular value decomposition. Thus, we endow the DMD algorithm with a randomized SVD algorithm aiming to improve the accuracy of the reduced order linear model and to reduce the CPU elapsed time. We gain a fast and accurate randomized DMD algorithm, exploiting an efficient low-rank DMD model of input data.

Algorithm 1 describes the procedure for computing the randomized SVD and it is adapted after Halko et al. [49].

Algorithm 1: Randomized SVD algorithm (RSVD)

Initial data: $V_0^{N-1} \in \mathbb{R}^{m \times n}$, $m \geq n$, integer target rank $k \geq 2$ and $k < n$.

1. Generate random matrix $M = \text{rand}(n, r)$, $r = \min(n, 2k)$.
2. Multiplication of snapshot matrix with random matrix $Q = V_0^{N-1}M$.
3. Orthogonalization $Q \leftarrow \text{orth}(Q)$.
4. Projection of snapshot matrix $V = Q^H V_0^{N-1}$, where H denotes the conjugate transpose.

5. Produce the economy size singular value decomposition $[Q_1, \Sigma, W] = \text{SVD}(V)$.

6. Compute the right singular vectors $U = QQ_1$.

Output: Procedure returns $U \in \mathbb{R}^{m \times k}$, $\Sigma \in \mathbb{R}^{k \times k}$, $W \in \mathbb{R}^{n \times k}$.

We define the relative error of the low-rank model as the L_2 -norm of the difference between the experimental variables and approximate DMD solutions over the exact one, that is,

$$Er_{DMD} = \frac{\|v(\mathbf{x}) - v_{DMD}(\mathbf{x})\|_2}{\|v(\mathbf{x})\|_2}, \quad (11)$$

where $v(\mathbf{x})$ represent the experimental data and $v_{DMD}(\mathbf{x})$ represent the low-rank DMD approximation.

The correlation coefficient defined below is used as additional metric to validate the quality of the low-rank DMD model:

$$C_{DMD} = \frac{(\|v(\mathbf{x}) \cdot v_{DMD}(\mathbf{x})\|_F)^2}{\|v(\mathbf{x})^H \cdot v(\mathbf{x})\|_F \|v_{DMD}(\mathbf{x})^H \cdot v_{DMD}(\mathbf{x})\|_F}, \quad (12)$$

where $v(\mathbf{x})$ means the experimental data, $v_{DMD}(x)$ represent the computed solution by means of the reduced order DMD model, (\cdot) represents the Hermitian inner product and H denotes the conjugate transpose. We denote by $\|\cdot\|_F$ the Frobenius matrix norm in the sense that for any matrix $A \in \mathbb{C}_{m \times n}$ having singular values $\sigma_1, \dots, \sigma_n$ and SVD of the form $A = U\Sigma V^H$, then

$$\|A\|_F = \|U^H A V\|_F = \|\Sigma\|_F = \sqrt{\sigma_1^2 + \dots + \sigma_n^2}. \quad (13)$$

The rank of the reduced DMD model is given such that the relative error of data reconstruction becomes sufficiently small and the correlation coefficient is sufficiently high. We recall this procedure as *adaptive randomized dynamic mode decomposition*. Determination of the optimal rank of the reduced DMD model then amounts to finding the solution to the following optimization problem:

$$\begin{cases} \text{Find } v_{DMD}^t(\mathbf{x}) = \sum_{j=1}^k a_j \phi_j(\mathbf{x}) \lambda_j^{t-1}, \\ \text{Subject to } k = \arg \min Er_{DMD} \text{ and } k = \arg \max C_{DMD}. \end{cases} \quad (14)$$

The adaptive randomized DMD algorithm (**Algorithm 2**) that we applied in the forthcoming section for data originating from the Saint-Venant system proceeds as follows:

Algorithm 2: Adaptive randomized DMD algorithm (ARDMD)

Initial data: $V_0^{N-1} \in \mathbb{R}^{m \times n}$, $V_1^N \in \mathbb{R}^{m \times n}$, $m \geq n$, integer target rank $k \geq 2$ and $k < n$.

1. Variate k .
2. Produce the randomized singular value decomposition: $[U, \Sigma, W] = \text{RSVD}(V_0^{N-1}, k)$, where U contains the proper orthogonal modes of V_0^{N-1} and Σ contains the singular values.
3. Solve the minimization problem (8): $S = U^H (V_1^N W \Sigma^{-1})$.

For the reader information we will detail it in the following. Relations $\mathcal{A}V_0^{N-1} = V_1^N = V_0^{N-1}S + R$, $\|R\|_2 \rightarrow 0$ and $V_0^{N-1} = U\Sigma W^H$ yield:

$$\begin{aligned} \mathcal{A}U\Sigma W^H &= V_1^N = U\Sigma W^H S \\ &\Rightarrow U^H \mathcal{A}U\Sigma W^H = U^H U\Sigma W^H S \\ &\Rightarrow S = U^H \mathcal{A}U. \end{aligned}$$

From $\mathcal{A}U\Sigma W^H = V_1^N$ it follows that $\mathcal{A}U = V_1^N W \Sigma^{-1}$ and hence $S = U^H (V_1^N W \Sigma^{-1})$.

4. Compute dynamic modes solving the eigenvalue problem $SX = X\Lambda$ and obtain dynamic modes as $\Phi = UX$. The diagonal entries of Λ represent the eigenvalues λ .

5. Project dynamic modes onto the first snapshot to calculate the vector containing dynamic modes amplitudes $Ampl = (a_j)_{j=1}^{rank(\Lambda)}$.
6. The DMD model of rank k is given by the product

$$V_{DMD} = \Phi \cdot diag(Ampl) \cdot Van, \quad (15)$$

where the Vandermonde matrix is

$$Van = \begin{pmatrix} 1 & \lambda_1^1 & \lambda_1^2 & \dots & \lambda_1^{N-2} \\ 1 & \lambda_2^1 & \lambda_2^2 & \dots & \lambda_2^{N-2} \\ 1 & \vdots & \vdots & \vdots & \vdots \\ \dots & \dots & \dots & \dots & \dots \\ 1 & \lambda_k^1 & \lambda_k^2 & \dots & \lambda_k^{N-2} \end{pmatrix}.$$

7. Solve the optimization problem (14) and obtain the optimal low rank k and associated V_{DMD} .
Output: k, V_{DMD} .

The first major advantage of the adaptive randomized DMD proposed in this paper is represented by the fact that **Algorithm 2** produces a reduced order subspace of Ritz values, having the same dimension as the rank of RSVD function. In consequence, after solving the optimization problem (14), an additional selection algorithm of the Ritz values associated with their DMD modes is no longer needed. We employ in the flow reconstruction the most influential DMD modes associated with their amplitudes and Ritz values, respectively, leading to the minimum error of flow reconstruction, due to the adaptive feature of the proposed algorithm.

The second major improvement offered by the proposed randomized DMD can be found in the significantly reduction of CPU time for computation of massive numerical data, as we will detail in the section dedicated to numerical results.

3. MULTIDIMENSIONAL RADIAL BASIS FUNCTION INTERPOLATION

3.1. Model-order reduction using projection

So far, the model order reduction practitioners applied the intrusive model order reduction having modal decomposition (POD or DMD) and the Galerkin projection compound.

In the Cartesian or Cylindrical coordinates formulation, we suppose there exists a time dependent flow $v = (\mathbf{x}, \mathbf{t}) \in \mathbb{V}$ and a given initial flow $v(\mathbf{x}, 0)$, that are solutions of the coupled system of nonlinear ordinary differential equations

$$\begin{cases} \frac{\partial v}{\partial t}(\mathbf{x}, \mathbf{t}) = f(t, v(\mathbf{x}, \mathbf{t})), \\ v(\mathbf{x}, \mathbf{t}_0) = v_0(\mathbf{x}), \end{cases} \quad (16)$$

obtained from the spatial discretization of evolution equations in continuous space.

To perform the intrusive model order reduction, we start by replacing the field v with v_{DMD} in (16) and project the resulting equations onto the subspace $X^{DMD} = span\{\phi_1(\cdot), \phi_2(\cdot), \dots, \phi_k(\cdot)\}$ spanned by the DMD basis to compute the following inner products:

$$\left\langle \phi_i(\cdot), \sum_{j=1}^k \lambda_j \phi_j(\cdot) \dot{a}_j(t) \right\rangle = \left\langle \phi_i(\cdot), f\left(t, \sum_{j=1}^k \lambda_j \phi_j(\cdot) a_j(t)\right) \right\rangle, \quad (17)$$

$$\left\langle \phi_i(\cdot), \sum_{j=1}^k \lambda_j \phi_j(\cdot) \dot{a}_j(t_0) \right\rangle = \langle \phi_i(\cdot), w_0 \rangle, \text{ for } i = 1, \dots, k, \quad (18)$$

where $\langle f, g \rangle = \int_{\Omega} f g d\Omega$.

The Galerkin projection gives the DMD-ROM, i.e., a dynamical system for temporal coefficients $\{a_j(t)\}_{j=1,\dots,k}$:

$$\dot{a}_i(t) = \left\langle \phi_i(\cdot), f\left(t, \sum_{j=1}^k \lambda_j \phi_j(\cdot) a_j(t)\right) \right\rangle, \quad (19)$$

with the initial condition

$$a_i(t_0) = \langle \phi_i(\cdot), v_0 \rangle, \text{ for } i = 1, \dots, k. \quad (20)$$

The resulting autonomous system has linear and quadratic terms parameterized by c_{im} , c_{imn} , respectively:

$$\dot{a}_i(t) = \sum_{m=1}^k \sum_{n=1}^k c_{imn} a_m(t) a_n(t) + \sum_{m=1}^k c_{im} a_m(t), \quad i = 1, \dots, k. \quad (21)$$

DMD in combination with the Galerkin projection method is an effective method for deriving a reduced order model. For a detailed description of this method, the reader is invited to consult our previous paper [32]. By projecting the full dynamical system onto a reduced space which is constructed based on the optimal DMD basis functions, the computational efficiency can be enhanced by several orders of magnitude. However, this approach presents several shortcomings. As in the case of POD-ROMs [38, 39, 40], this method implies analytical calculations and it remains dependent on the governing equations of the full physical system, therefore is not applicable in case of non-intrusive (or experimental) data.

Recently, a diversity of non-intrusive methods have been introduced into ROMs, associated so far with proper orthogonal decomposition, like: Smolyak sparse grid method [50], radial basis functions interpolation [51, 52, 53] or the method of generalized moving least squares [54].

In this paper we propose a novel approach to derive a reduced order model for non-intrusive data. In the offline stage of the proposed technique, the method of randomized dynamic mode decomposition finds the subspace $X^{DMD} = \text{span}\{\phi_1(\cdot), \phi_2(\cdot), \dots, \phi_k(\cdot)\}$ spanned by the sequence of the most efficient DMD modes. In the online stage, we involve the effectual multidimensional radial basis function interpolation who elegantly approximate the values of temporal coefficients for new time instances.

3.2. Model-order reduction by radial basis function interpolation

Since it was introduced by Rolland Hardy in 1970 [55] for applications in cartography, radial basis function (RBF) method has undergone a rapid progress as an active tool of mathematical interpolation of scattered data in many application domains like domain decomposition [56], unsteady fluid flows modelling [51, 4] or image processing [57]. Investigations upon accuracy and stability of RBF based interpolation may be found in Fornberg and Wright [58], Fasshauer [59] and Chenoweth [60].

The ARDMD algorithm previously described allows the identification of a reduced order model of form

$$v_{DMD}^t(\mathbf{x}) = \sum_{j=1}^k a_j \phi_j(\mathbf{x}) \lambda_j^{t-1}, \quad \lambda_j = e^{(\sigma_j + i\omega_j)\Delta t}, \quad t = t_1, \dots, t_N, \quad (22)$$

in which $\phi_j \in \mathbb{C}$ represents dynamic DMD modes, λ_j are the Ritz values, $a_j \in \mathbb{C}$ represent the modal amplitudes and k is the truncation order.

In the following, we employ the method of RBF interpolation, as a generalization of Hardy's multiquadric and inverse multiquadric method [61], for numerical interpolation of the model coefficients $b_j^t = a_j \lambda_j^{t-1}$ for $t \in [t_1, t_N]$.

Considering the determined coefficients as a set of distinct nodes $\{\mathbf{x}_i\}_{i=1}^{k \times N} \subset \mathbb{R}^2$ and a set of function values $\{f_i\}_{i=1}^{k \times N} \subset \mathbb{R}$, the problem reduces to find an interpolant $s: \mathbb{R}^2 \rightarrow \mathbb{R}$ such that

$$s(\mathbf{x}_i) = f_i \quad \text{for } i = 1, \dots, k \times N, \quad (23)$$

where N is the number of time instances for which experimentally measured data are available and k is the number of retained DMD modes. Note that we use the notation $f_i = b_j^t$, $j = 1, \dots, k$, $t = t_1, \dots, t_N$ for scattered points values and $\mathbf{x} = (x, y) \in \{1, \dots, k\} \times [t_1, t_N]$ for scattered points coordinates.

Considering $BL_2(\mathbb{R}^2)$ the Beppo-Levi space [62] of distributions on \mathbb{R}^2 with square integrable second derivatives, equipped with the rotation invariant semi-norm

$$\|s(\mathbf{x})\|^2 = \int_{\mathbb{R}^2} \left(\frac{\partial^2 s(\mathbf{x})}{\partial x^2} \right)^2 + \left(\frac{\partial^2 s(\mathbf{x})}{\partial y^2} \right)^2 + 2 \left(\frac{\partial^2 s(\mathbf{x})}{\partial x \partial y} \right)^2 d\mathbf{x} \quad (24)$$

we seek the smoothest interpolant surface in the affine space

$$S_{BL} = \{s \in BL_2(\mathbb{R}^2) \mid s(\mathbf{x}_i) = f_i, \quad i = 1, \dots, k \times N\}, \quad (25)$$

i.e.,

$$\tilde{s}(\mathbf{x}) = \arg \min_{s \in S_{BL}} \|s(\mathbf{x})\|^2. \quad (26)$$

The semi-norm (24) measures the energy or "smoothness" of the surface interpolant s , such that interpolants having a small semi-norm are considered smoother than those having a large semi-norm. Following Duchon [63] and Green and Silverman [64], the solution to the problem (26) is a function of the form

$$\tilde{s}(\mathbf{x}) = c_0 + c_1 \mathbf{x} + \sum_{i=1}^{k \times N} \beta_i K(\|\mathbf{x} - \mathbf{x}_i\|_2), \quad (27)$$

where K is a real valued function defined on the kernel $K \in \mathcal{K} : \mathbb{R}^{k \times N} \times \mathbb{R}^{k \times N} \rightarrow \mathbb{R}$, $\|\cdot\|_2$ is the Euclidian distance between the points \mathbf{x} and \mathbf{x}_i , the coefficients $\beta_i \in \mathbb{R}$ are constant real numbers and $\mathcal{P}(\mathbf{x}) = c_0 + c_1 \mathbf{x}$ is a global polynomial function, usually considered of small degree. The points \mathbf{x}_i are referred as centers of the Radial Basis Functions $K(r) = \mathcal{K}(\mathbf{x}, \mathbf{x}_i)$, where the variable r stands for $\|\mathbf{x} - \mathbf{x}_i\|_2$.

In our approach we use the so called *thinplate* kernel $K(r) = r^2 \ln(r+1)$. Ensuring that the interpolation surface lies in the Beppo-Levi space $\tilde{s} \in BL_2(\mathbb{R}^2)$ implies the following side conditions

$$\sum_{i=1}^{k \times N} \beta_i = \sum_{i=1}^{k \times N} x_i \beta_i = \sum_{i=1}^{k \times N} y_i \beta_i = 0 \quad (28)$$

and the constraints

$$\sum_{i=1}^{k \times N} \beta_i \mathcal{P}(\mathbf{x}_i) = 0. \quad (29)$$

Considering that $\{p_1, p_2\}$ represents a basis for the polynomial \mathcal{P} and $\{c_0, c_1\}$ are the coefficients that give the polynomial $\mathcal{P}(\mathbf{x})$ in terms of this basis, the interpolation conditions (23) with the side conditions (28) and constraints (29) lead to the following linear system to be solved for the coefficients that specify the RBF

$$\begin{pmatrix} K & P \\ P^T & 0 \end{pmatrix} \begin{pmatrix} \beta \\ c \end{pmatrix} = \begin{pmatrix} f \\ 0 \end{pmatrix}, \quad (30)$$

where $K_{ij} = K(\|\mathbf{x}_i - \mathbf{x}_j\|_2)$, $i, j = 1, \dots, k \times N$, $P_{ij} = p_j(\mathbf{x}_i)$, $i = 1, \dots, k \times N$, $j = 1, 2$, $\beta = (\beta_1, \dots, \beta_{k \times N})^T$, $c = (c_0, c_1)^T$, $f = (f_1, \dots, f_{k \times N})^T$. The zeros in (30) denote matrices or vectors of appropriate dimensions and 'T' stands for the transpose of a matrix or vector. Solving the linear system (30) determines the constant coefficients β and the polynomial coefficients c and hence the interpolant surface $\tilde{s}(\mathbf{x})$.

The methodology presented herein leads to the following linear model (denoted in the following ARDMD-RBF model) for estimation of the flow field for any time instance $t \in [t_1, t_N]$

$$v_{DMD}^t(\mathbf{x}) = \sum_{j=1}^k b_j^t \phi_j(\mathbf{x}), \quad b_j^t = \tilde{s}(\mathbf{x}_i), \quad \mathbf{x}_i \in \{1, \dots, k\} \times [t_1, t_N], \quad (31)$$

where b_j^t are the interpolated coefficients, $\phi_j(\mathbf{x})$ are the DMD basis functions, k represents the number of the DMD basis functions retained for the reduced order model and t denotes any value of time in the interval $[t_1, t_N]$.

4. ANALYSIS OF THE REDUCED ORDER MODEL FOR SAINT-VENANT DATA

4.1. Acquisition of numerical data

The test problem used in this paper is consisting of the nonlinear Saint Venant equations model (also called the shallow water equations [33]) in a channel on the rotating earth, associated with periodic boundary conditions in the \tilde{x} -direction and solid wall boundary condition in the \tilde{y} -direction:

$$\tilde{u}_{\tilde{t}} + \tilde{u}\tilde{u}_{\tilde{x}} + \tilde{v}\tilde{u}_{\tilde{y}} + (g\tilde{h})_{\tilde{x}} - \tilde{f}\tilde{v} = 0, \quad (32)$$

$$\tilde{v}_{\tilde{t}} + \tilde{u}\tilde{v}_{\tilde{x}} + \tilde{v}\tilde{v}_{\tilde{y}} + (g\tilde{h})_{\tilde{y}} + \tilde{f}\tilde{u} = 0, \quad (33)$$

$$(g\tilde{h})_{\tilde{t}} + (g\tilde{h}\tilde{u})_{\tilde{x}} + (g\tilde{h}\tilde{v})_{\tilde{y}} = 0, \quad (34)$$

$$\tilde{u}(0, \tilde{y}, \tilde{t}) = \tilde{u}(L_{\max}, \tilde{y}, \tilde{t}), \quad \tilde{v}(\tilde{x}, 0, \tilde{t}) = \tilde{v}(\tilde{x}, D_{\max}, \tilde{t}) = 0, \quad (35)$$

where \tilde{u} and \tilde{v} are the velocity components in the \tilde{x} and \tilde{y} axis directions respectively, $g\tilde{h}$ is the geopotential height, \tilde{h} represents the depth of the fluid, \tilde{f} is the Coriolis factor and g is the acceleration of gravity. We consider that the reference computational configuration is the rectangular $2D$ domain $\Omega = [0, L_{\max}] \times [0, D_{\max}]$. Subscripts represent the derivatives with respect to time and the streamwise and spanwise coordinate.

The Saint Venant equations have been used for a wide variety of hydrological and geophysical fluid dynamics phenomena such as tide-currents [65], pollutant dispersion [66], storm-surges or tsunami wave propagation [37]. Early work on numerical methods for solving the shallow water equations is described in Navon (1979) [67].

We consider the model (32)-(35) in a β -plane assumption detailed in [68], in which the effect of the Earth's sphericity is modeled by a linear variation in the Coriolis factor

$$\tilde{f} = f_0 + \frac{\beta}{2}(2\tilde{y} - D_{\max}), \quad (36)$$

where f_0, β are constants, L_{\max}, D_{\max} are the dimensions of the rectangular domain of integration.

The following initial condition introduced by Grammelvedt [69] was adopted as the initial height field which propagates the energy in wave number one, in the streamwise direction:

$$h_0(\tilde{x}, \tilde{y}) = H_0 + H_1 \tanh\left(\frac{9(D_{\max}/2 - \tilde{y})}{2D_{\max}}\right) + H_2 \sin\left(\frac{2\pi\tilde{x}}{L_{\max}}\right) \cosh^{-2}\left(\frac{9(D_{\max}/2 - \tilde{y})}{D_{\max}}\right). \quad (37)$$

Using the geostrophic relationship $\tilde{u} = -\tilde{h}_{\tilde{y}}(g/\tilde{f})$, $\tilde{v} = \tilde{h}_{\tilde{x}}(g/\tilde{f})$, the initial velocity fields are derived as:

$$u_0(\tilde{x}, \tilde{y}) = -\frac{g}{\tilde{f}} \frac{9H_1}{2D_{\max}} \left(\tanh^2\left(\frac{9D_{\max}/2 - 9\tilde{y}}{2D_{\max}}\right) - 1 \right) - \frac{18g}{\tilde{f}} H_2 \sinh\left(\frac{9D_{\max}/2 - 9\tilde{y}}{D_{\max}}\right) \frac{\sin\left(\frac{2\pi\tilde{x}}{L_{\max}}\right)}{D_{\max} \cosh^3\left(\frac{9D_{\max}/2 - 9\tilde{y}}{D_{\max}}\right)}, \quad (38)$$

$$v_0(\tilde{x}, \tilde{y}) = 2\pi H_2 \frac{g}{\tilde{f} L_{\max}} \cos\left(\frac{2\pi\tilde{x}}{L_{\max}}\right) \cosh^{-2}\left(\frac{9(D_{\max}/2 - \tilde{y})}{D_{\max}}\right). \quad (39)$$

The dimensional constants used for the above test model are

$$f_0 = 10^{-4} s^{-1}, \quad \beta = 1.5 \times 10^{-11} s^{-1} m^{-1}, \quad g = 10 m s^{-1},$$

$$D_{\max} = 44 \times 10^5 \text{m}, \quad L_{\max} = 6 \times 10^6 \text{m}, \quad H_0 = 2 \times 10^6 \text{m}, \quad H_1 = 220 \text{m}, \quad H_2 = 133 \text{m}. \quad (40)$$

We have followed the approach used by Navon [70], which implements a two-stage finite-element Numerov-Galerkin method for integrating the nonlinear shallow-water equations on a β -plane limited-area domain, for approximating the quadratic nonlinear terms that appear in the equations of hydrological dynamics. This scheme when applied to meteorological and oceanographic problems gives an accurate phase propagation and also handles nonlinearities well. The accuracy of temporal and spatial discretization equals $\mathcal{O}(k^2, h^p)$, where p varies in the interval [4, 8]. The training data comprises a number of 240 unsteady solutions of the two-dimensional shallow water equations model (32)–(39), at regularly spaced time intervals $\Delta t = 600 \text{s}$ for each solution variable.

To measure the accuracy of the reduced shallow water model and to validate the numerical results with existing results in the literature, we undertake a non-dimensional analysis of the shallow water model. Following [71], reference quantities of the dependent and independent variables in the shallow water model are considered, i.e. the length scale $L_{ref} = L_{\max}$ and the reference units for the height and velocity, respectively, are given by the initial conditions $h_{ref} = h_0$, $u_{ref} = u_0$. A typical time scale is also considered, assuming the form $t_{ref} = L_{ref}/u_{ref}$. In order to make the system of equations (32)–(35) non-dimensional, we define the non-dimensional variables

$$(t, x, y) = (\tilde{t}/t_{ref}, \tilde{x}/L_{ref}, \tilde{y}/L_{ref}), \quad (h, u, v) = (\tilde{h}/h_{ref}, \tilde{u}/u_{ref}, \tilde{v}/u_{ref}).$$

The numerical results are obtained and used in further numerical experiments in dimensionless form.

4.2. Advantages of ARDMD algorithm over classic approaches

In this section, the efficiency of reduced order modelling based on the ARDMD algorithm is illustrated in comparison with the classic DMD algorithm, considering the evolution of the flow field along the integration time window. The first major advantage of the adaptive randomized DMD proposed in this work is represented by the fact that the ARDMD algorithm produces a reduced order subspace of Ritz values, which has the same dimension as the rank of randomized SVD function. In consequence, this procedure omits a further selection of the Ritz values associated with their DMD modes.

In case of the classic DMD algorithm, the superposition of all Koopman modes approximates the entire data sequence, but there are also modes that have a weak contribution. The modes' selection, which is central in model reduction, constitutes the source of many discussions among modal decomposition practitioners. For instance, Jovanovic et al. [72] introduced a low-rank DMD algorithm to identify an a-priori specified number of modes that provide optimal approximation of experimental or numerical snapshots at a certain time interval. Consequently, the modes and frequencies that have strongest influence on the quality of approximation have been selected. An optimized DMD method was recently introduced by Chen et al. [14], which tailors the decomposition to a desired number of modes. This method minimizes the total residual over all data vectors and uses simulated annealing and quasi-Newton minimization iterative methods for selecting the frequencies. Tissot and his coworkers [73] propose a new energetic criterion for model reduction using Dynamic Mode Decomposition, that incorporates the growth rate of the modes.

To highlight the efficiency of the ARDMD method presented herein, we illustrate in Figures 1–3 the spectra of DMD decomposition of geopotential height field h , streamwise field u and spanwise field v , respectively, in case of the new ARDMD algorithm and the classic DMD algorithm which was applied in [47].

Obviously, when the classic DMD algorithm is applied, the practitioner has to address a modes' selection method like those mentioned above. Instead, the randomized DMD algorithm (ARDMD) produces a significantly reduced size spectrum which elegantly incorporates the most influential modes. Figures 4–6 present an insight of how ARDMD works. The optimization problem (14) is solved using a simulated annealing optimization routine which is detailed in [74], based on sequential quadratic programming (SQP) [75]. This leads to the optimal low rank k and associated DMD subspace V_{DMD} where the most influential DMD bases live. The rank of the reduced DMD

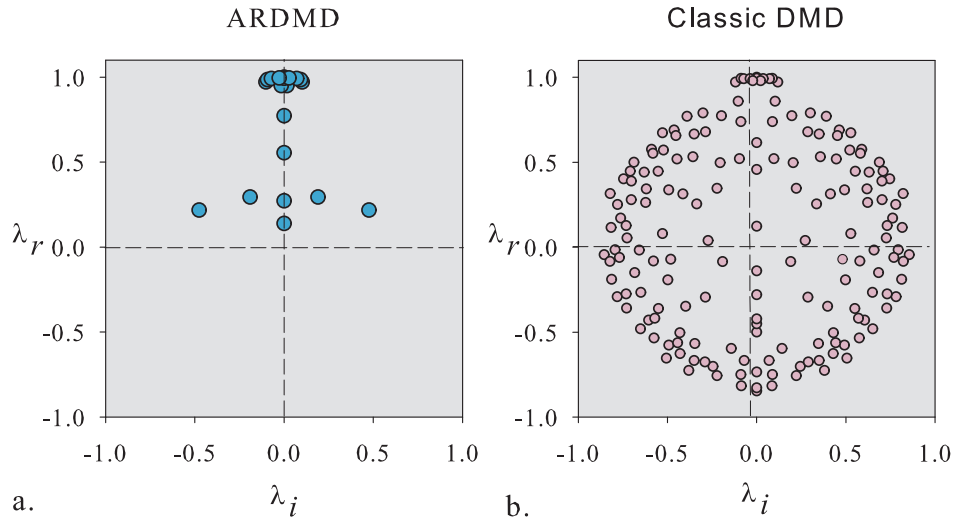


Figure 1. The spectrum of DMD decomposition of geopotential height field h in case of: a) ARDMD algorithm used in the present paper, b) classic DMD algorithm used in [47].

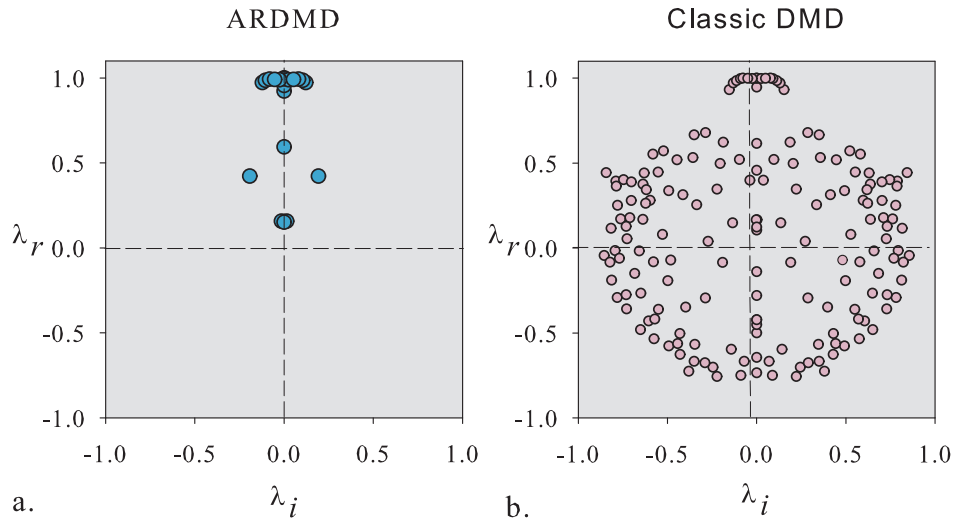


Figure 2. The spectrum of DMD decomposition of streamwise field u in case of: a) ARDMD algorithm used in the present paper, b) classic DMD algorithm used in [47].

model is automatically found such that the relative error of field reconstruction given by Eq. (11) becomes sufficiently small and the correlation coefficient (12) is sufficiently high. The optimal rank of the reduced DMD model is the unique solution to the optimization problem (14). ARDMD algorithm produces subspaces of order $k = 20$ selected from 173 DMD modes. A significant reduction of a factor of eight and a half is achieved for the representation of Saint-Venant fields h , u and v .

The ARDMD algorithm presented herein is fully capable of determining the modal growth rates and the associated frequencies, which are illustrated in Figure 7 for velocity fields u , v , respectively. This is of major importance when is necessary to isolate modes with very high amplitudes at lower frequencies or high frequency modes having lower amplitudes.

The numerical results provided by the ARDMD algorithm are presented in Table I.

A comparison of the reduced order modelling rank, in the case of several DMD based modal decomposition methods associated with certain modes' selection criteria proposed in our previous

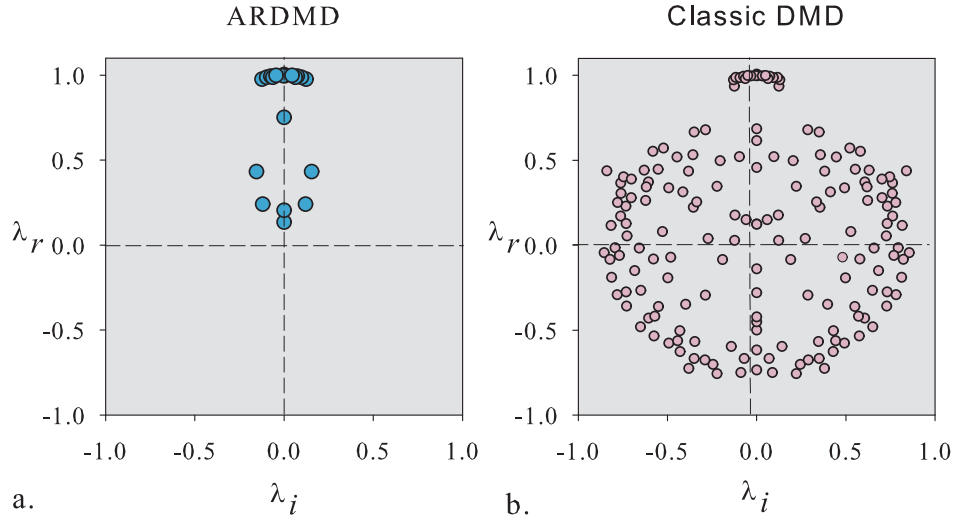


Figure 3. The spectrum of DMD decomposition of spanwise field v in case of: a) ARDMD algorithm used in the present paper, b) classic DMD algorithm used in [47].

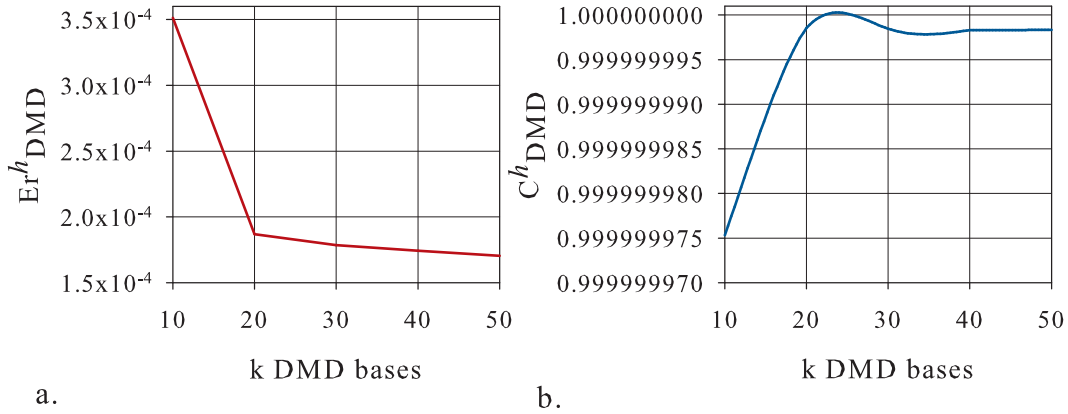


Figure 4. The process of evaluation of ROM target rank for h field: a) The relative error of ARDMD computed as the retained number of dynamic modes, b) The correlation coefficient of ARDMD computed as the retained number of dynamic modes.

Table I. The relative error Er_{DMD} , the correlation coefficient C_{DMD} and the reduced order modelling rank k obtained from ARDMD modal decomposition.

| Flow field | The relative error | The correlation coefficient | The ROM rank |
|------------|--------------------------------------|-----------------------------|--------------|
| $h(x, y)$ | $Er^h_{DMD} = 1.7909 \times 10^{-4}$ | $C^h_{DMD} = 0.99999$ | $k = 20$ |
| $u(x, y)$ | $Er^u_{DMD} = 1.4738 \times 10^{-3}$ | $C^u_{DMD} = 0.99999$ | $k = 20$ |
| $v(x, y)$ | $Er^v_{DMD} = 4.5316 \times 10^{-3}$ | $C^v_{DMD} = 0.99999$ | $k = 20$ |

ARDMD, adaptive randomized dynamic mode decomposition, ROM, reduced order model.

investigations and novel ARDMD technique is presented in Table II. Ref. [32] aimed to present a preliminary survey on DMD modes selection. We proposed a framework for modal decomposition of 2D flows, when numerical or experimental data are captured with large time steps. Key

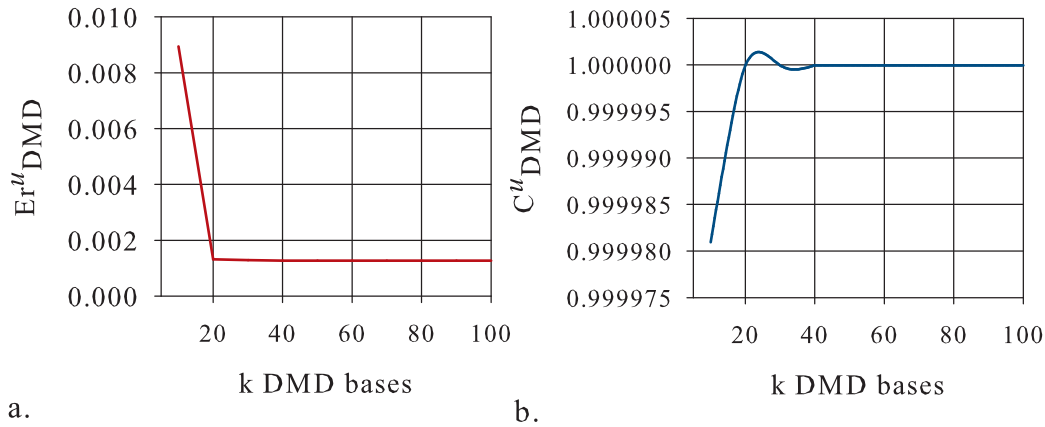


Figure 5. The process of evaluation of ROM target rank for u field: a) The relative error of ARDMD computed as the retained number of dynamic modes, b) The correlation coefficient of ARDMD computed as the retained number of dynamic modes.

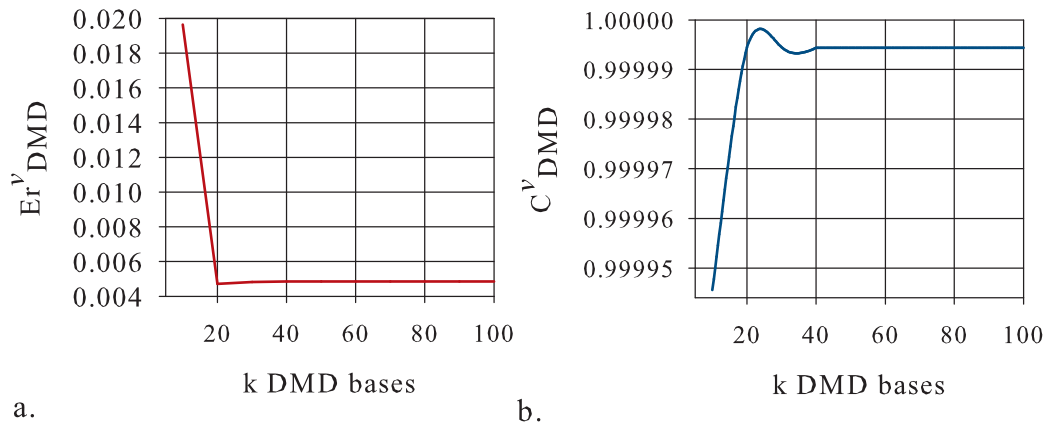


Figure 6. The process of evaluation of ROM target rank for v field: a) The relative error of ARDMD computed as the retained number of dynamic modes, b) The correlation coefficient of ARDMD computed as the retained number of dynamic modes.

innovations for the DMD-based ROM introduced in [32] are the use of the Moore-Penrose pseudoinverse in the DMD computation that produced an accurate result and a novel selection method for the DMD modes. Unlike the classic algorithm, we arrange the Koopman modes in descending order of the energy of the DMD modes weighted by the inverse of the Strouhal number. We eliminate the modes that contribute weakly to the data sequence based on the conservation of quadratic integral invariants [76] by the reduced order flow. The resulting optimization problem was solved by employing sequential quadratic programming (SQP) [75].

In [25] we proposed a new framework for dynamic mode decomposition based on the reduced Schmid operator. We investigated a variant of DMD algorithm and we explored the selection of the modes based on sorting them in decreasing order of their amplitudes. This procedure works well for models without modes that are very rapidly damped, having very high amplitudes. Therefore the selection of modes based on their amplitude is effective only in certain situations, as reported also by Noack et al. [21].

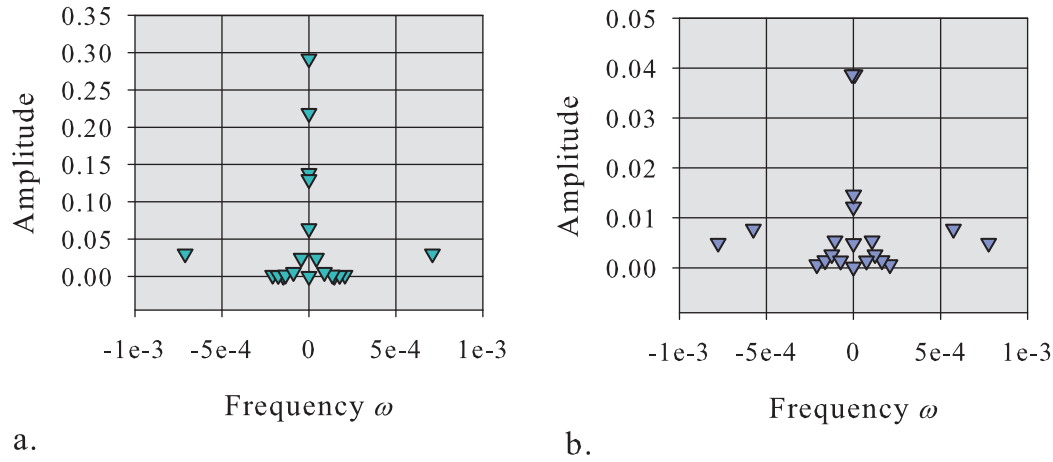


Figure 7. The amplitudes of DMD modes and associated frequencies obtained by dynamic mode decomposition of streamwise velocity field u (a) and spanwise velocity field v (b).

The investigation recently presented in [47] has focused on the effects of modes selection in dynamic mode decomposition. We proposed a new vector filtering criterion for dynamic modes selection that is able to extract dynamically relevant flow features of time-resolved experimental or numerical data. The algorithm related in [47] proposed a dynamic filtering criterion for which the amplitude of any mode is weighted by its growth rate. This method proved to be perfectly adapted to the flow dynamics, in identification of the most influential modes.

Table II. The reduced order modelling rank k and the relative error Er^h_{DMD} in case of several DMD based modal decomposition methods.

| energetic DMD ([32]) | reduced Schmid operator DMD ([25]) | dynamic DMD ([47]) | ARDMD algorithm the present research |
|-----------------------|------------------------------------|-------------------------|--------------------------------------|
| 13 | 19 | 11 | 20 |
| 1.19×10^{-3} | 2.683×10^{-4} | 2.5785×10^{-4} | 1.7909×10^{-4} |

DMD, dynamic mode decomposition, ARDMD, adaptive randomized dynamic mode decomposition.

Data presented in Table II argues the efficiency of the novel ARDMD method. Although the previous techniques detailed in [32, 25, 47] lead to a reduced number of retained modes, there are still missing modes that would contribute to data approximation. Hence the relative error of flow reconstruction by the reduced order model is the best in the case of randomized dynamic mode decomposition. Producing a slightly larger model rank k than the previous algorithms, the great advantage of adaptive randomized DMD (ARDMD) is that omits the efforts of implementing an additional criterion of influential modes' selection, they being selected automatically.

Thus a significant reduction in computational time is also achieved. The CPU time gained by applying several DMD techniques is presented in Figure 8. By employing the ARDMD algorithm in comparison with dynamic DMD [47] and energetic DMD [32], the computational complexity of the reduced order model is diminished from the very beginning by two times and three times, respectively, as illustrated in Figure 8.

Estimation of low order model coefficients by interpolation, in cases of non-intrusive data, represent a cost effective solution, as has been also reported in the literature by Raisee et al. [77], Peherstorfer and Willcox [78], Lin et al. [79]. The coefficients of the reduced order models

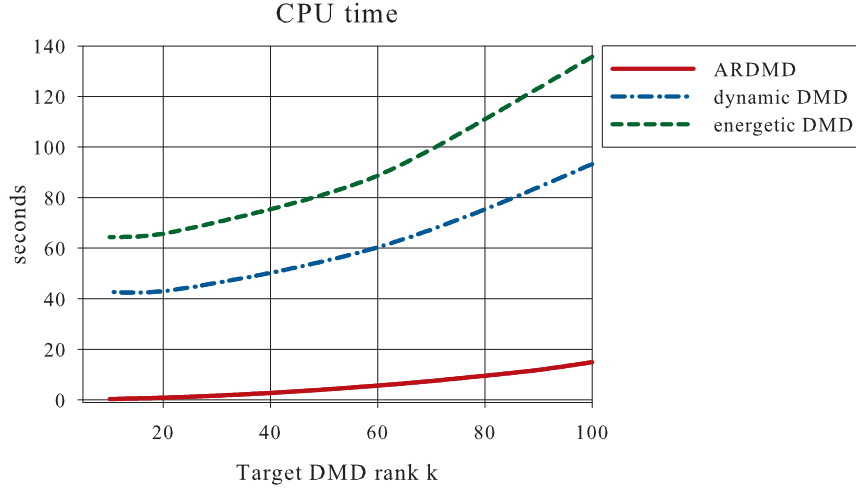


Figure 8. CPU time gained by applying several DMD techniques: ARDMD, adaptive randomized dynamic mode decomposition (present research), dynamic DMD method presented in [47], energetic DMD method employed in [32].

of state solutions $(h_{DMD}, u_{DMD}, v_{DMD})(x, y)$ have been estimated for entire time window by interpolating the DMD computed coefficients using radial basis functions (RBF) discussed in Section 3. They are depicted in Figure 9.

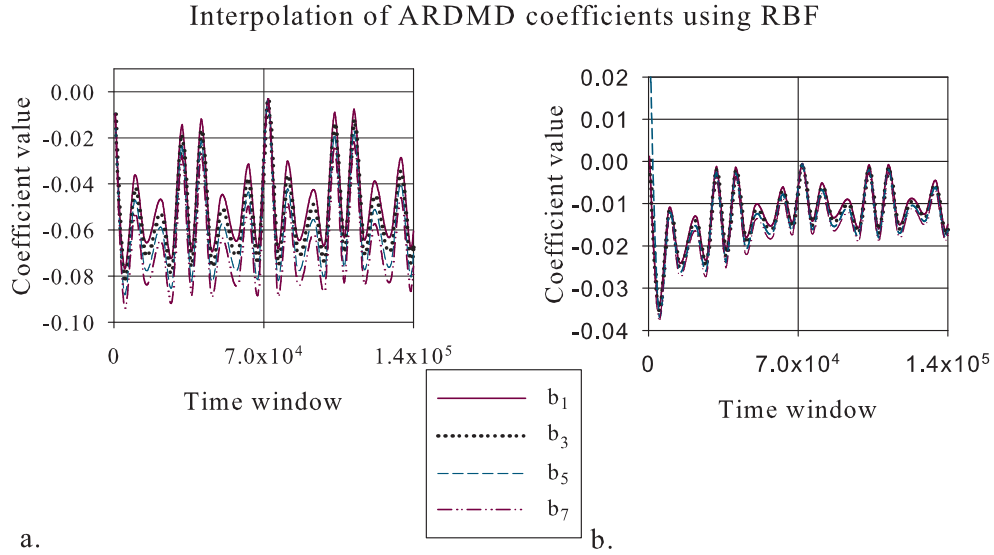


Figure 9. The coefficients of the reduced order models (a) $h_{DMD}(x, y)$ and (b) $u_{DMD}(x, y)$ obtained by radial basis functions (RBF) interpolation, $b_j = a_j \lambda_j^{t-1}$ for $j = 1, \dots, k$.

Using the ARDMD algorithm, we obtain the non-intrusive reduced order models (NIROMs) of the state solutions $(h, u, v)(x, y, t)$. The validity of the methodology introduced in this paper is checked by comparing how the NIROMs assess the full solution fields given by the experimental data at time instance 181, in Figures 10 and 11, respectively. We applied a normalization condition such that the maximum amplitude of the physical components $(h, u, v)(x, y, t)$ fields over the (x, y) stations is unity. The NIROM models employ the Ritz values represented in Figures 1-3 and associated DMD modes and amplitudes determined by the ARDMD algorithm.

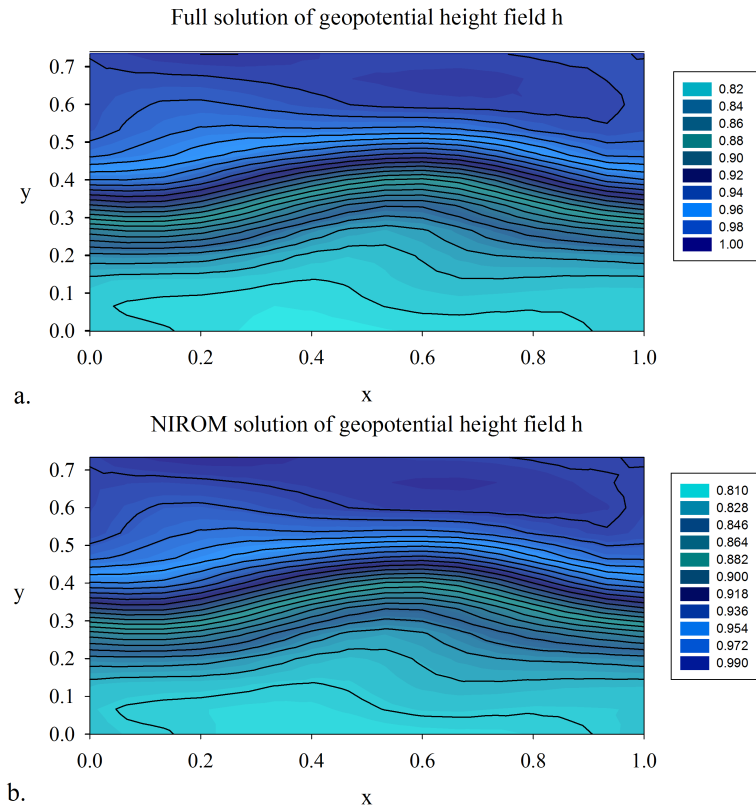


Figure 10. a) Full solution of geopotential height field; b) NIROM solution of geopotential height field.

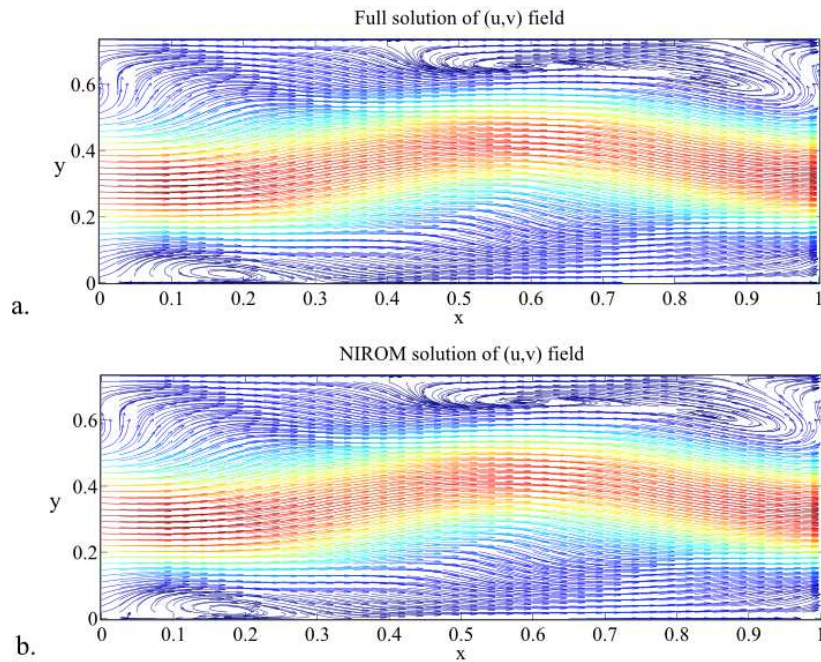


Figure 11. a) Full solution of (u, v) field; b) NIROM solution of (u, v) field.

The local error between the full SWE solution and NIROM solution, respectively, at time instance 181 is provided in Figure 12.

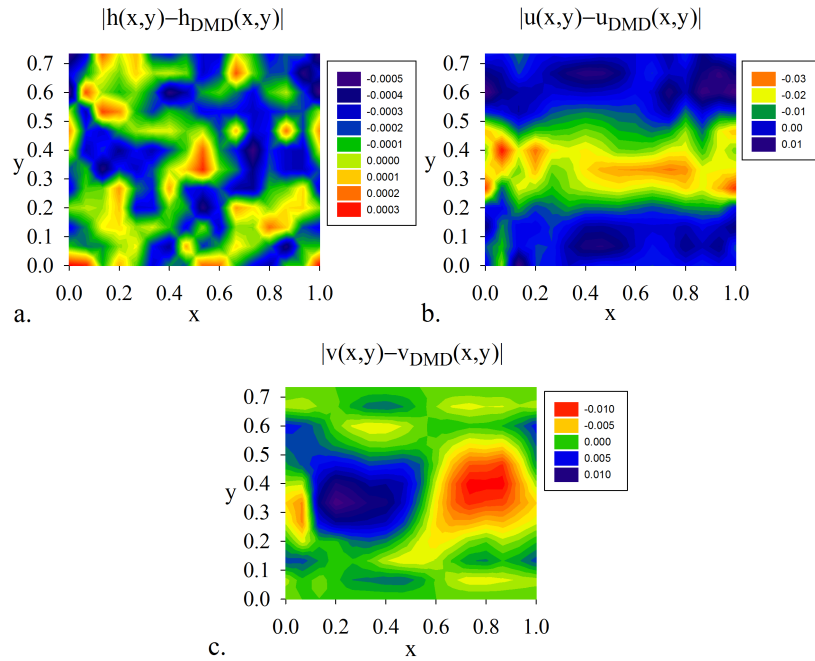


Figure 12. Local error between full SWE solution and NIROM of geopotential height field (a), NIROM of streamwise velocity field (b), NIROM of spanwise velocity field (c), respectively.

The coherent structures in the (u, v) field can be visualized as local vortices in the first DMD modes, which are illustrated in Figure 13 and Figure 14.

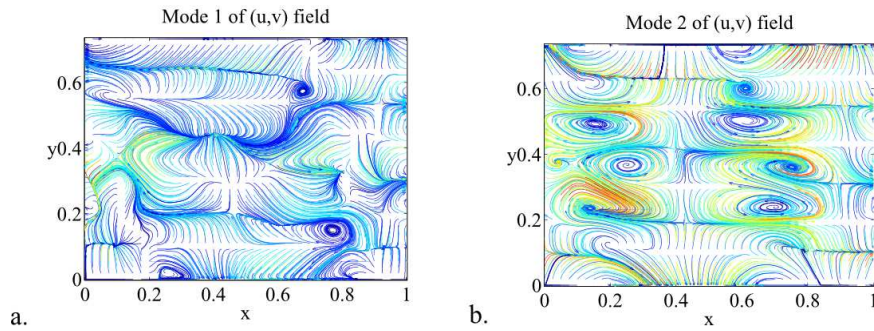


Figure 13. The first two DMD modes of the (u, v) field.

The flow reconstructions by non-intrusive reduced order models (NIROMs) presented in Figure 10 and Figure 11 are very close to experimental data snapshots, comparing the solution of SWE flow field after 181 steps. The values of the correlation coefficients provided in Table I greater than 99% confirm the validity of the NIROMs. The similarity between the characteristics of the flow field and those obtained by the NIROMs validates the method presented here and certifies that the improved ARDMD method can be applied successfully to model reduction of 2D flows.

For the problem investigated here, the novel ARDMD method shows satisfactory performances and provides a higher degree of accuracy for flow linear reduced order model.

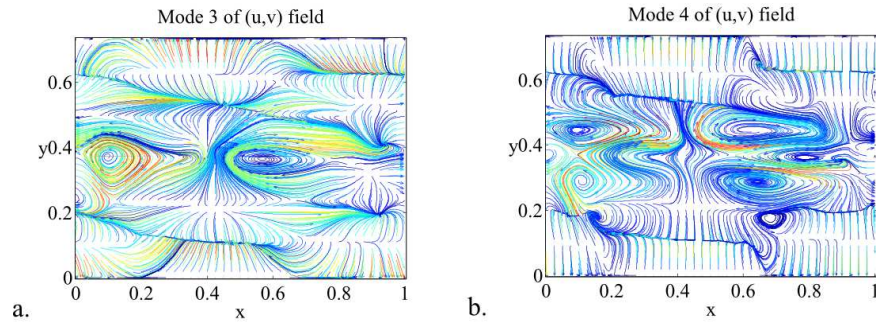


Figure 14. The third and fourth DMD modes of the (u, v) field.

5. SUMMARY AND CONCLUSIONS

In this paper we have proposed a framework for reduced order modelling of non-intrusive data with application to 2D flows. To overcome the inconveniences of intrusive model order reduction usually derived by combining the POD and the Galerkin projection methods, we developed a novel technique based on randomized dynamic mode decomposition as a fast and accurate option in model order reduction of non-intrusive data originating from Saint-Venant systems. We derived a non-intrusive approach to obtain a reduced order linear model of the flow dynamics based on dynamic mode decomposition of experimental data in association with the efficient radial basis function interpolation technique.

To the best of our knowledge, the present paper is the first work that introduced the randomized dynamic mode decomposition algorithm with application to fluid dynamics, after the randomized SVD algorithm recently introduced by Erichson and Donovan [41] for processing of high resolution videos.

Several key innovations have been introduced in the present paper:

- We endow the dynamic mode decomposition (DMD) algorithm with a randomized singular value decomposition (RSVD) algorithm.
- We gain a fast and accurate adaptive randomized DMD algorithm (ARDMD), exploiting an efficient low rank DMD model of input data.
- The rank of the reduced DMD model is given as the unique solution of an optimization problem whose constraints are a sufficiently small relative error of data reconstruction and a sufficiently high correlation coefficient between the experimental data and the DMD solution.

The major advantages of the adaptive randomized dynamic mode decomposition (ARDMD) proposed in this work are:

- This method provides an efficient tool in developing the linear model of a complex flow field described by non-intrusive (or experimental) data.
- This method does not require an additional selection algorithm of the DMD modes. ARDMD produces a reduced order subspace of Ritz values, having the same dimension as the rank of randomized SVD function, where the most influential DMD modes live.
- We gain a significantly reduction of CPU time in computation of ROMs for massive numerical data.
- Combining the randomized dynamic mode decomposition with radial basis function (RBF) interpolation we have derived a reduced order model for estimating the flow behavior in the real time window. The non-intrusive reduced order model (NIROM) presents satisfactory performances in flow reconstruction.
- Analyzing the modal growth rates and the associated frequencies is an instance of apprehending the flow dynamics. This is of major importance when is necessary to isolate modes with very high amplitudes at lower frequencies or high frequency modes having lower

amplitudes. Thus this paper outlines steps towards hydrodynamic stability analysis and flow control with potential applications.

To highlight the performances of the proposed methodology we performed a comparison of the reduced order modelling rank, in the case of several DMD based modal decomposition methods associated with certain modes selection criteria and novel ARDMD technique presented herein. The numerical results argued the efficiency of the novel ARDMD method.

We emphasized the excellent behavior of the NIROMs developed in this paper by comparing the computed shallow water solution with the experimentally measured profiles and we found a close agreement. In addition, we performed a qualitative analysis of the reduced order models by correlation coefficients and local errors.

There are a number of interesting directions that arise from this work. First, it will be a natural extension to apply the proposed algorithm to high-dimensional data originating from fluid dynamics and oceanographic/atmospheric measurements. The methodology presented here offers the main advantage of deriving a reduced order model capable to provide a variety of information describing the behavior of the flow field. A future extension of this research will address an efficient numerical approach for modal decomposition of swirling flows, where the full mathematical model implies more sophisticated relations at domain boundaries that must be satisfied by the reduced order model also.

REFERENCES

1. Chevreuil M, Nouy A. Model order reduction based on proper generalized decomposition for the propagation of uncertainties in structural dynamics. *International Journal for Numerical Methods in Engineering* 2011; **89**(2):241–268.
2. Stefanescu R, Navon IM. POD/DEIM nonlinear model order reduction of an ADI implicit shallow water equations model. *Journal of Computational Physics* 2013; **237**:95–114.
3. Dimitriu G, Stefanescu R, Navon IM. POD-DEIM approach on dimension reduction of a multi-species host-parasitoid system. *Annals of the Academy of Romanian Scientists, Mathematics and its Applications* 2015; **7**(1):173–188.
4. Xiao D, Fang F, Pain C, Hu G. Non-intrusive reduced-order modelling of the Navier-Stokes equations based on RBF interpolation. *International Journal for Numerical Methods in Fluids* 2015; **79**(11):580–595.
5. Du J, Fang F, Pain CC, Navon IM, Zhu J, Ham D. POD reduced order unstructured mesh modelling applied to 2D and 3D fluid flow. *Computers and Mathematics with Applications* 2013; **65**:362–379.
6. Fang F, Pain CC, Navon IM, Cacuci DG, Chen X. The independent set perturbation method for efficient computation of sensitivities with applications to data assimilation and a finite element shallow water model. *Computers and Fluids* 2013; **76**:33–49.
7. Cao Y, Zhu J, Luo Z, Navon IM. Reduced order modeling of the upper tropical Pacific ocean model using proper orthogonal decomposition. *Computers and Mathematics with Applications* 2006; **52**(8-9):1373–1386.
8. Cao Y, Zhu J, Navon I, Luo Z. A reduced order approach to four-dimensional variational data assimilation using proper orthogonal decomposition. *International Journal for Numerical Methods in Fluids* 2007; **53**(10):1571–1583.
9. Chen X, Navon IM, Fang F. A dual-weighted trust-region adaptive POD 4D-VAR applied to a finite-element shallow-water equations model. *International Journal for Numerical Methods in Fluids* 2011; **65**:250–541.
10. Stefanescu R, Sandu A, Navon IM. POD/DEIM reduced-order strategies for efficient four dimensional variational data assimilation. *Journal of Computational Physics* 2015; **295**:569–595.
11. Bialecki RA, Fic AJKA. Proper orthogonal decomposition and modal analysis for acceleration of transient FEM thermal analysis. *International Journal for Numerical Methods in Engineering* 2004; **62**(6):774–797.
12. Carlberg K, Bou-Mosleh C, Farhat C. Efficient non-linear model reduction via a least-squares PetrovGalerkin projection and compressive tensor approximations. *International Journal for Numerical Methods in Engineering* 2011; **86**(2):155–181.
13. Semaan R, Kumar P, Burnazzi M, Tissot G, Cordier L, Noack BR. Reduced-order modelling of the flow around a high-lift configuration with unsteady Coanda blowing. *Journal of Fluid Mechanics* 2016; **800**:72–110.
14. Chen KK, Tu JH, Rowley CW. Variants of dynamic mode decomposition: boundary condition, Koopman and Fourier analyses. *Nonlinear Science* 2012; **22**:887–915.
15. Rowley CW, Mezic I, Bagheri S, Schlatter P, Henningson DS. Spectral analysis of nonlinear flows. *Journal of Fluid Mechanics* 2009; **641**:115–127.
16. Schmid P. Dynamic mode decomposition of numerical and experimental data. *Journal of Fluid Mechanics* 2010; **656**:5–28.
17. Golub G, van Loan CF. *Matrix Computations, Third Edition*. The Johns Hopkins University Press, 1996.
18. Schmid PJ, Sesterhenn J. Dynamic mode decomposition of numerical and experimental data. *61st Annual Meeting of the APS Division of Fluid Dynamics*, vol. 53(15), American Physical Society: San Antonio, Texas, 2008.
19. Koopman B. Hamiltonian systems and transformations in Hilbert space. *Proc. Nat. Acad. Sci.* 1931; **17**:315–318.
20. Schmid PJ, Meyer KE, Pust O. Dynamic mode decomposition and proper orthogonal decomposition of flow in a lid-driven cylindrical cavity. *8th International Symposium on Particle Image Velocimetry - PIV09*, 2009.

21. Noack BR, Morzynski M, Tadmor G. *Reduced-Order Modelling for Flow Control*. Springer, 2011.
22. Bagheri S. Koopman-mode decomposition of the cylinder wake. *Journal of Fluid Mechanics* 2013; **726**:596–623.
23. Rowley CW, Mezic I, Bagheri S, Schlatter P, Henningson DS. Reduced-order models for flow control: balanced models and Koopman modes. *Seventh IUTAM Symposium on Laminar-Turbulent Transition, IUTAM Bookseries*, vol. 18, 2010; 43–50.
24. Frederich O, Luchtenburg DM. Modal analysis of complex turbulent flow. *The 7th International Symposium on Turbulence and Shear Flow Phenomena (TSFP-7)*, Ottawa, Canada., 2011.
25. Alekseev AK, Bistrian DA, Bondarev AE, Navon IM. On linear and nonlinear aspects of dynamic mode decomposition. *International Journal for Numerical Methods in Fluids* 2016; DOI: **10.1002/ld.4221**.
26. Seena A, Sung HJ. Dynamic mode decomposition of turbulent cavity flows for self-sustained oscillations. *International Journal of Heat and Fluid Flow* 2011; **32**:10981110.
27. Hua JC, Gunaratne GH, Talley DG, Gord JR, Roy S. Dynamic-mode decomposition based analysis of shear coaxial jets with and without transverse acoustic driving. *Journal of Fluid Mechanics* 2016; **790**:5–32.
28. Mezic I. Spectral properties of dynamical systems, model reduction and decompositions. *Nonlinear Dynamics* 2005; **41**(1-3):309–325.
29. Mezic I. Analysis of fluid flows via spectral properties of the Koopman operator. *Annual Review of Fluid Mechanics* 2013; **45**(1):357–378.
30. Bagheri S. Computational hydrodynamic stability and flow control based on spectral analysis of linear operators. *Archives of Computational Methods in Engineering* 2012; **19**(3):341–379.
31. Brunton SL, Brunton BW, Proctor JL, Kutz JN. Koopman invariant subspaces and finite linear representations of nonlinear dynamical systems for control. *PLoS ONE* 2016; **11**(2):e0150171, doi:10.1371/journal.pone.0150171.
32. Bistrian DA, Navon IM. An improved algorithm for the shallow water equations model reduction: Dynamic mode decomposition vs POD. *International Journal for Numerical Methods in Fluids* 2015; **78**(9):552–580.
33. Vreugdenhil C. *Numerical Methods for Shallow Water Flow*. Kluwer Academic Publishers, 1994.
34. Galdi G. *An Introduction to the Mathematical Theory of the Navier-Stokes Equation*. Springer, 1994.
35. Gilman P. Magnetohydrodynamic “shallow water” equations for the solar tachocline. *The Astrophysical Journal Letters* 2000; **554**:L79L82.
36. Bouchut F, Lhebrard X. A 5-wave relaxation solver for the shallow water MHD system. *Journal of Scientific Computing* 2016; **68**:92–115.
37. Koutitus C. *Mathematics models in coastal engineering*. Pentech Press: London, 1988.
38. Amsallem D, Farhat C. Stabilization of projection-based reduced-order models. *International Journal for Numerical Methods in Engineering* 2011; **91**(4):358–377.
39. San O, Iliescu T. A stabilized proper orthogonal decomposition reduced-order model for large scale quasigeostrophic ocean circulation. *Advances in Computational Mathematics* 2014; **41**(5):12891319.
40. Ballarin F, Manzoni A, Quarteroni A, Rozza G. Supremizer stabilization of POD-Galerkin approximation of parametrized steady incompressible Navier-Stokes equations. *International Journal for Numerical Methods in Engineering* 2015; **102**(5):1136–1161.
41. Erichson NB, Donovan C. Randomized low-rank Dynamic Mode Decomposition for motion detection. *Computer Vision and Image Understanding* 2016; **146**:40–50.
42. Belson B, Tu JH, Rowley CW. Algorithm 945: Modred - a parallelized model reduction library. *ACM Transactions on Mathematical Software* 2014; **40**(4):Article 30.
43. Williams MO, Kevrekidis IG, Rowley CW. A data-driven approximation of the Koopman operator: extending dynamic mode decomposition. *Nonlinear Science* 2015; 1–40; doi:10.1007/s00332-015-9258-5.
44. Chopra AK. *Dynamics of Structures*. 4th edition, Prentice-Hall International Series in Civil Engineering and Engineering Mechanics, 2000.
45. Noack BR, Stankiewicz W, Morzynski M, Schmid P. Recursive dynamic mode decomposition of a transient cylinder wake. *physics.flu-dyn arXiv:1511.06876v1*, 2015.
46. Kutz JN, Fu X, Brunton SL, Erichson NB. Multi-resolution dynamic mode decomposition for foreground/background separation and object tracking. *2015 IEEE International Conference on Computer Vision Workshop (ICCVW)*, INSPEC Accession Number:15790263, IEEE: Santiago, 2015; 921 – 929.
47. Bistrian DA, Navon IM. The method of dynamic mode decomposition in shallow water and a swirling flow problem. *International Journal for Numerical Methods in Fluids* 2016; DOI: **10.1002/ld.4257**.
48. Fiedler M. A note on companion matrices. *Linear Algebra and its Applications* 2003; **372**:325–331.
49. Halko N, Martinsson PG, Tropp JA. Finding structure with randomness: Probabilistic algorithms for constructing approximate matrix decompositions. *SIAM Review* 2011; **53**(2):2017–288.
50. Xiao D, Lin Z, Fang F, Pain CC, Navon IM, Salinas P, Muggeridge A. Non-intrusive reduced-order modeling for multiphase porous media flows using Smolyak sparse grids. *International Journal for Numerical Methods in Fluids* 2016; doi:10.1002/ld.4263.
51. Walton S, Hassan O, Morgan K. Reduced order modelling for unsteady fluid flow using proper orthogonal decomposition and radial basis functions. *Applied Mathematical Modelling* 2013; **37**:8930–8945.
52. Bistrian DA, Susan-Resiga RF. Weighted proper orthogonal decomposition of the swirling flow exiting the hydraulic turbine runner. *Applied Mathematical Modelling* 2016; **40**:4057–4078.
53. Xiao D, Yang P, Fang F, Pain CC, Navon IM. Non-intrusive reduced order modelling of fluid structure interactions. *Computer Methods in Applied Mechanics and Engineering* 2016; **303**:35–54.
54. Dehghan M, Mohammadi V. Two numerical meshless techniques based on radial basis functions (RBFs) and the method of generalized moving least squares (GMLS) for simulation of coupled Klein-Gordon-Schrodinger (KGS) equations. *Computers and Mathematics with Applications* 2016; **71**:892–921.
55. Hardy RL. Multiquadric equations of topography and other irregular surfaces. *Journal of Geophysical Research* 1970; **76**(8):1905–1915.
56. Beatson RK, Light WA, Billings S. Fast solution of the radial basis function interpolation equations: Domain decomposition methods. *SIAM Journal of Scientific Computing* 2000; **22**(5):1717–1740.

57. Carr JC, Beatson RK, Cherrie JB, Mitchell TJ, Fright WR, McCallum BC, Evans TR. Reconstruction and representation of 3d objects with radial basis functions. *ACM SIGGRAPH* 2001; **2001**:67–76.
58. Fornberg B, Wright G. Stable computation of multiquadric interpolants for all values of the shape parameter. *Computers and Mathematics with Applications* 2004; **48**:853–867.
59. Fasshauer GE. *Meshfree Approximation Methods with MATLAB*. World Scientific Publishers, 2007.
60. Chenoweth ME. A numerical study of generalized multiquadric radial basis function interpolation. *SIAM Undergraduate Research Online* 2009; **2**:58–70.
61. Hardy RL. Theory and applications of the multiquadric-biharmonic method: 20 years of discovery. *Computers and Mathematics with Applications* 1990; **19**:163–208.
62. Aikawa H. *Potential Theory*, chap. On weighted Beppo Levi functions. Springer US, 1988; 1–6.
63. Duchon J. *Constructive Theory of Functions of Several Variables*, vol. Lecture Notes in Mathematics, chap. Splines minimizing rotation-invariant semi-norms in Sobolev spaces. Springer-Verlag., 1977; 85–100.
64. Green PJ, Silverman BW. *Nonparametric Regression and Generalized Linear Models: A roughness penalty approach*. 1 edition, Chapman and Hall/CRC, 1993.
65. Bryden IG, Couch SJ, Owen A, Melville G. Tideequations resource assessment. *Proc. IMechE Part A: Journal of Power and Energy* 2007; **221**:125–135.
66. Sportisse B, Djouad R. Reduction of chemical kinetics in air pollution modeling. *Journal of Computational Physics* 2000; **164**:354–376.
67. Navon IM. Finite-element simulation of the shallow-water equations model on a limited area domain. *Applied Mathematical Modeling* 1979; **3**:337–348.
68. Navon I. A Numerov-Galerkin technique applied to a finite-ement shallow water equations model with enforced conservation of integral invariants and selective lumping. *Journal of Computational Physics* 1983; **52**:313–339.
69. Grammelvedt A. A survey of finite-difference schemes for the primitive equations for a barotropic fluid. *Monthly Weather Review* 1969; **97**(5):384–404.
70. Navon IM. Feudx: A two-stage, high accuracy, finite-element Fortran program for solving shallow-water equations. *Computers and Geosciences* 1987; **13**(3):255–285.
71. Barenblatt GI. *Scaling, self-similarity and intermediate asymptotics*. Cambridge Texts in Applied Mathematics. Cambridge University Press: Cambridge, New York, Melbourne, 1996.
72. Jovanovic MR, Schmid PJ, Nichols JW. Low-rank and sparse dynamic mode decomposition. *Center for Turbulence Research Annual Research Briefs* 2012; :139–152.
73. Tissot G, Cordier L, Benard N, Noack BR. Model reduction using dynamic mode decomposition. *Comptes Rendus Mecanique* 2014; **342**:410–416.
74. Yang XS. *Engineering Optimization: An Introduction with Metaheuristic Applications*. Wiley, USA, 2010.
75. Nocedal J, Wright SJ. *Numerical Optimization*. Second edition, Springer, 2006.
76. Navon IM, DeVilliers R, Gustaf R. A quasi-Newton nonlinear ADI Fortran IV program for solving the shallow-water equations with augmented Lagrangians. *Computers and Geosciences* 1986; **12**:151–173.
77. Rasee M, Kumar D, Lacor C. A non-intrusive model reduction approach for polynomial chaos expansion using proper orthogonal decomposition. *International Journal for Numerical Methods in Engineering* 2015; **103**(4):293312.
78. Peherstorfer B, Willcox K. Data-driven operator inference for nonintrusive projection-based model reduction. *Computer Methods in Applied Mechanics and Engineering* 2016; **306**:196–215.
79. Lin Z, Xiao D, Fang F, Pain C, Navon IM. Non-intrusive reduced order modelling with least squares fitting on a sparse grid. *International Journal for Numerical Methods in Fluids* 2016; doi:10.1002/flid.4268.